Design and Performance Analysis of Frequency-Shift Keyed Transmitter using Rapidly Tunable Lasers

by

Carol Pan
S.B., Electrical Engineering and Computer Science, Massachusetts Institute of Technology (2022)

Submitted to the Department of Electrical Engineering and Computer Science

in partial fulfillment of the requirements for the degree of
Master of Engineering in Electrical Engineering and Computer Science

at the
MASSACHUSETTS INSTITUTE OF TECHNOLOGY

June 2023

DISTRIBUTION STATEMENT A. Approved for public release. Distribution is unlimited.

This material is based upon work supported under Air Force Contract No. FA8702-15-D-0001. Any opinions, findings, conclusions or recommendations expressed in this material are those of the author(s) and do not necessarily reflect the views of the U.S. Air Force.

Authored by: Carol Pan
Department of Electrical Engineering and Computer Science
May 12, 2023

Certified by: Jeffrey M. Roth
Technical Staff, MIT Lincoln Laboratory
Thesis Supervisor

Certified by: Jelena Notaros
Assistant Professor
Thesis Supervisor

Accepted by: Katrina LaCurts
Chair, Master of Engineering Thesis Committee

Design and Performance Analysis of Frequency-Shift Keyed Transmitter using Rapidly Tunable Lasers

by

Carol Pan

Submitted to the Department of Electrical Engineering and Computer Science
on May 12, 2023, in partial fulfillment of the
requirements for the degree of
Master of Engineering in Electrical Engineering and Computer Science

Abstract

Optical Frequency Shift Keying (FSK) is a modulation scheme that encodes data in the wavelength of a carrier signal. Due to the large amount of optical bandwidth available in the erbium, 1.55-μm telecom band, FSK can potentially utilize a wide spectrum to achieve multi-Gb/s channel bandwidths. For free-space laser communication (lasercom) applications, links are usually point-to-point, have narrow beamwidths, and do not need to share a transmitting medium with other signals. Therefore, many lasercom applications could exploit the benefits of FSK by trading off spectral efficiency with power efficiency. This thesis investigates an FSK transmitter implementation utilizing a single, fast tunable laser, allowing scalability to high values of M-ary FSK, where M represents the number of wavelengths in the symbol constellation. This work will propose and implement a design for an FSK-modulated transmitter using a modulated-grating, y-branch tunable laser, and assess its suitability for lasercom applications.

Thesis Supervisor: Jeffrey M. Roth
Title: Technical Staff, MIT Lincoln Laboratory

Thesis Supervisor: Jelena Notaros
Title: Assistant Professor

Acknowledgments

I would like to extend my sincerest gratitude towards my Lincoln Laboratory advisor and supervisor, Jeffrey Roth, for his guidance and support both in the inspiration of my interest in this field, as well as in the formulation of my thesis. Thank you also to Brandon John, who helped me with my microcontroller woes in a time when official Arduino documentation insisted on lying to me, and who, unknowingly, provided the sample thesis that helped me put this paper together.

I also wish to thank Jeffrey Minch, Tim Yarnall, Craig Langois, and Vincent Scalesse for all of their direction and aid with both the larger and finer details, and the use of their vast technical repertoire. Finally, I especially would like to thank my advisor, Prof. Jelena Notaros, for all of her help in facilitating the resources needed and all the advice she generously imparted in the facilitation of my thesis year.

This thesis could not come to fruition without the immense support from MIT Lincoln Laboratory and MIT. Thank you!

Contents

List of Figures

List of Tables

Chapter 1

Introduction

The ongoing growth in bandwidth requirements for communications has been driving improved technologies that can extend both transmission distance and bandwidth. In the optical domain, terrestrial telecom has been adopting 100 Gb/s+ technologies to support increased internet traffic. The field of free-space laser communications (lasercom) is also enabling a growing number of optical links between satellites to achieve multi-Gb/s connectivity between mobile platforms [1, 2]. For these lasercom systems, links must function over long distances with high range losses, and are usually single, point-to-point links. Therefore, power efficiency is often of higher importance than spectral efficiency, due to the need to transmit as much information as possible per photon of energy.

1.1 Modulation Schemes

In digital communications, a signal carrier is modulated with a symbol that contains information. The symbol can be encoded in the amplitude of the carrier, the frequency, the phase, polarization, or a combination of all four. A given symbol can encode one or more bits of information. Accordingly, the information transfer over a channel is represented by the bit rate, which can be represented as:

$$\text{Bit Rate} = \text{Symbol Rate} \times \text{Number of Bits per Symbol}.$$

The bit rate refers to the number of bits transmitted per second, the symbol rate is defined as how many symbols are transmitted per second, and the number of bits per symbol can be mathematically written as $\log_2$(Number of Unique Symbols). In free-space laser communications, waveforms that provide highest receiver sensitivity and that can transmit the maximum amount of information per symbol help achieve the highest link efficiencies.

1.1.1 Amplitude Modulation

Amplitude modulation is a basic category of modulation techniques that use discretized amplitude measurements of a signal to convey information. In amplitude shift keying (ASK), information is determined based on the strength of a given signal. On-off keying (OOK) is a basic form of AM where a symbol is either a pulse or an empty time slot, allowing for one bit of information per symbol. More complicated forms of amplitude modulation using graduated power levels allow multiple bits of information to be coded per symbol, but such waveforms are easily degraded by intensity noise or fluctuations. Optical systems often implement intensity modulation, which is a subset of amplitude modulation and stems from the receiver process that performs a square-law detection on the optical field, thereby measuring intensity (or power) at the receiver.

1.1.2 Pulse-Position Modulation

A form of amplitude modulation is pulse-position modulation (PPM), which encodes using time position instead of pulse strength. PPM transmits a short pulse at a specific subset within a slot time that is matched to the symbol rate. The slot time can be divided into multiple subsets of time, and the number of subsets determines the constellation of symbols possible for each bit. In theory, such a modulation scheme can be scaled by arbitrarily reducing the size of the encoding time slots to indefinitely increase the number of symbols. However, in practice the number of bits encoded in every symbol becomes limited by factors such as electrical bandwidth, timing syn-

chronization accuracy, and nonlinearities [4]. PPM comes closest to the current limits of achieving high-M-ary modulation schemes with amplitude-modulation approaches. PPM serves as a good benchmark for the performance comparison for other high-M-ary modulation approaches.

1.1.3 Phase-Shift Keying

Phase-shift keying is a common modulation approach that has been extensively used in RF communications, and is now becoming common in optical systems. This modulation scheme outputs a continuous laser signal and relies on discrete changes in phase to encode information. A large benefit of this modulation is that it has a much larger signal-to-noise ratio (SNR) due to the introduction of a quadrature axis, and is accordingly more power efficient. However, most PSK systems require a more complex demodulation scheme requiring a local oscillator (LO) laser. Differential phase-shift keying (DPSK) is a subset of PSK, and allows self frequency referencing using a simple delay-line interferometer rather than a local oscillator, but has a performance penalty of approximately 3 dB over a fully coherent PSK approach.

1.1.4 Frequency Shift Keying

This paper proposes an implementation of a multiple frequency shift keying (M-FSK) modulation scheme. FSK uses discrete changes in frequency to encode bit information within an optical communication link, and can achieve higher receiver sensitivity and increased immunity to noise compared to OOK. Optical FSK can achieve high symbol constellations without requiring excessive electrical bandwidth in either the transmitter or receiver, which is the case with PPM. The power efficiency with FSK also is equivalent to that for PPM. An FSK-modulated waveform requires a large optical bandwidth relative to other modulation approaches, which is usually not a significant driver for lasercom applications that typically have less constrained channel bandwidths.

Laser transmitters operating in the 1.55-μm band (200-THz regime) might target a

difference in wavelength symbols in the picometer range, corresponding to MHz-scale symbol spacings. The total receiver bandwidth for this class of high-symbol M-FSK system (M$\geq$256) can be in the 10-GHz range, which is well within the electrical bandwidth of a typical photo-receiver [4]. However, scaling of the FSK approach to high-symbol M-FSK system constellations becomes challenging if using discrete lasers, due to excessive amounts of power consumption and hardware complexity. The use of conventional, fixed-frequency lasers in M-FSK would require multiple lasers operating simultaneously, greatly increasing the power consumption of such a system.

The channel capacity, or the maximum rate data can be transmitted over a noisy channel and remain error-free, is shown in Fig. 1-2 for M-FSK systems. This model assumes hard-decision receiver logic and incoherent detection, and is useful in comparing theoretical performance in different modulation systems [3]. On the opposite end, Fig. 1-3 displays the efficiency of a proposed M-FSK system, or the cost (in power) to achieve one of the maximum data rates calculated in the preceding figure.

Fig. 1-4 demonstrates how the efficiency of a 16-FSK system compares against widely-used modulation formats demodulated using their default receiver types. For OOK, this is photon-counting. For PPM and DPSK, this is a heterodyne incoherent receiver. Finally, we perform one more comparison with the 16-FSK coherent receiver and the 16-FSK incoherent receiver. Note that PPM and FSK have very similar efficiencies.

1.2 Tunable Lasers

Tunable lasers can provide an alternative approach to implementing FSK waveforms, utilizing electronic control to change wavelength. Advancements have allowed tunable lasers to be controlled across a larger tuning range than previously achievable, and at low enough latency and response times that could support high-speed communications. The modulated-grating, y-branch tunable laser (MG-YTL) device architecture, for example, can achieve fast, 3-ns tuning within the same super-mode [5] with a tuning range comprising entire C-band (approximately 191.2 THz to 196.0 THz) using

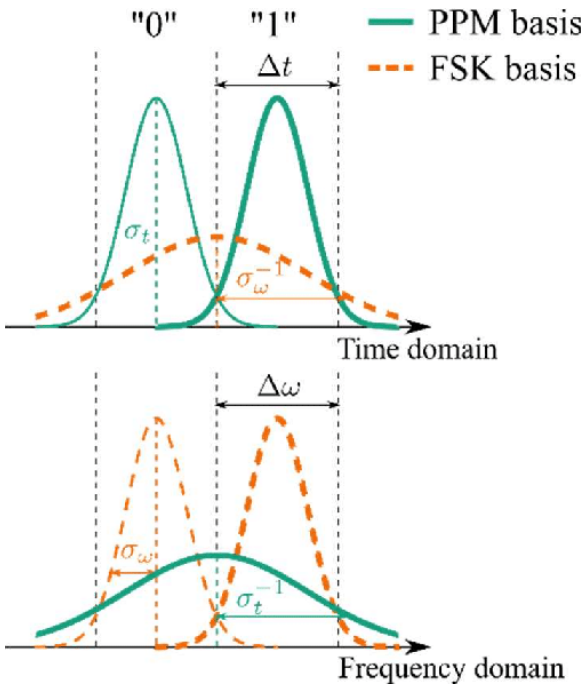

Figure 1-1: Simplified comparison of PPM and FSK in the frequency and time domain, where σ_t and σ_ω refer to the standard deviation in the time and frequency domains, respectively. Rödiger, Jasper & Perlot, Nicolas & Benson, Oliver & Freund, Ronald, *Time-frequency Quantum Key Distribution over a Free-Space Optical Link* (2021); licensed under a Creative Commons Attribution (CC BY) license.

current control. Existing digital-to-analog converters (DACs) can switch the control currents at up to 1.56 MHz [6]. This thesis investigates the efficiency and performance of a M-FSK modulation scheme implemented with a Finisar S7500 MG-YTL commercial device.

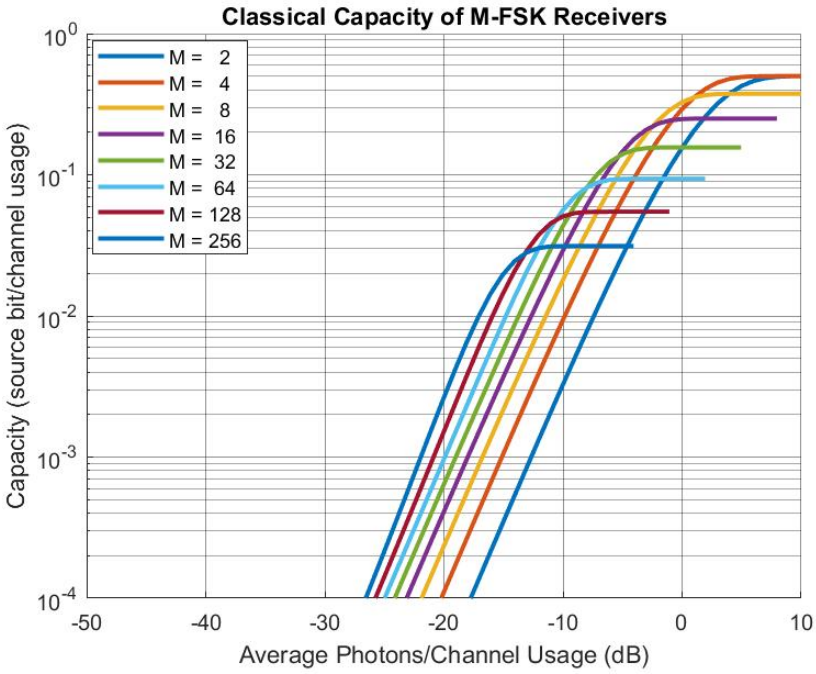

Figure 1-2: Channel capacity curves for M-FSK receivers using heterodyne incoherent hard decision.

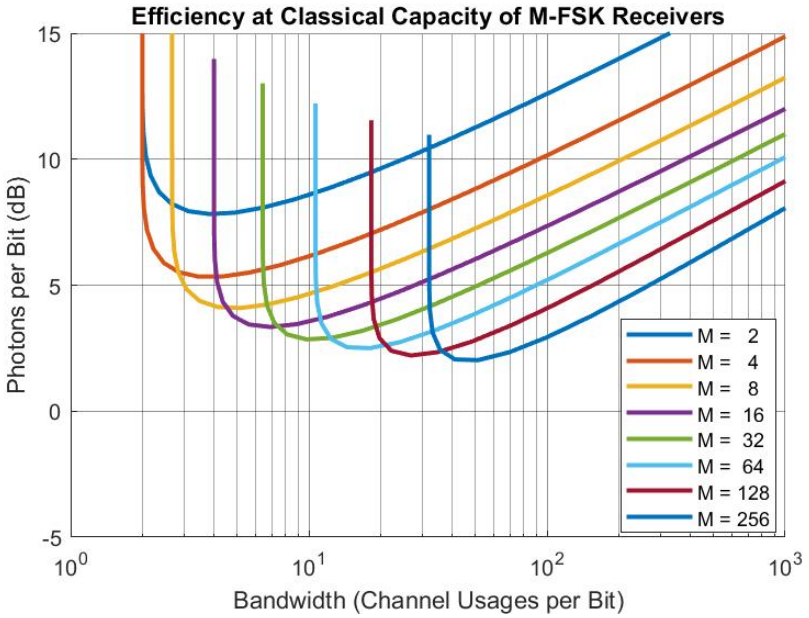

Figure 1-3: Efficiency curve at classical capacity for M-FSK receivers using heterodyne incoherent hard decision.

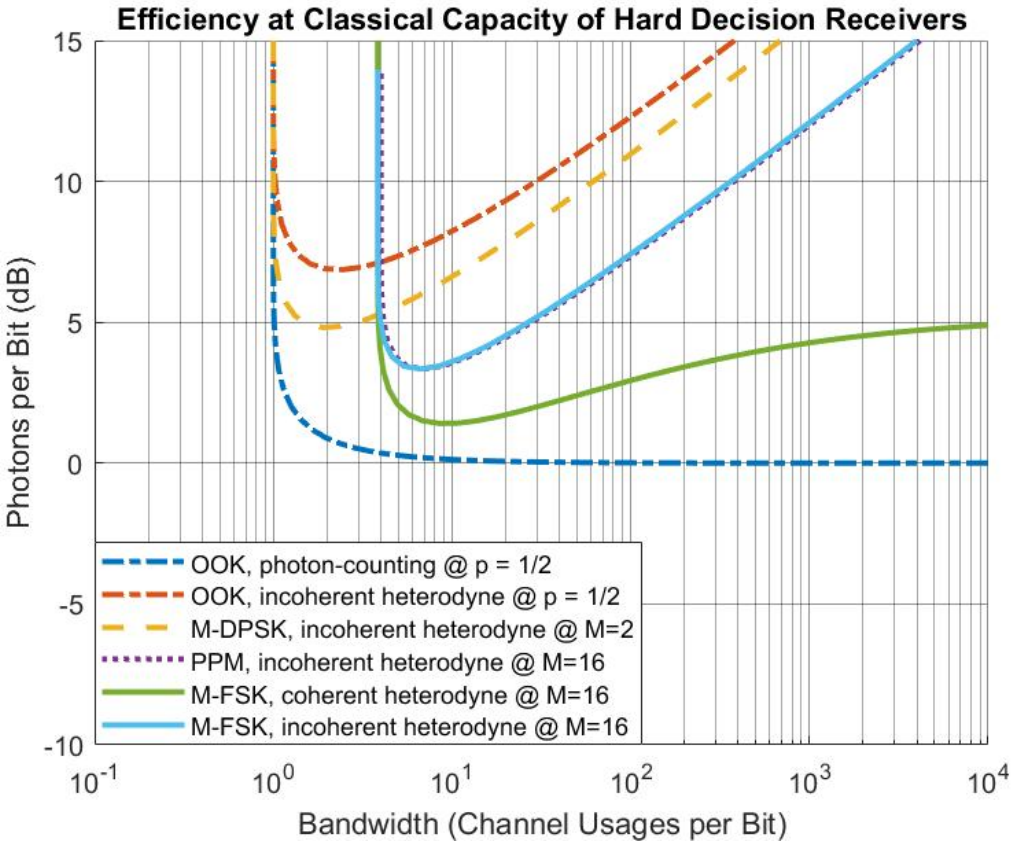

Figure 1-4: Efficiency curves at classical capacity for conventional modulation formats and corresponding hard-decision receivers.

Chapter 2

System Specifications and Design

This chapter covers the design rationale and subsequent implementation of a high-M-ary FSK transmitter based on a rapidly-tunable MG-YTL laser. Section 2.1 details the design decisions involved in the physical creation of a transmitter and presents the resulting performance characteristics. Section 2.2 describes how to properly transmit a digital signal using the implemented transmitter.

2.1 Transmitter Specifications

Section 2.1.1 covers the hardware design of the high-M-ary FSK transmitter. Section 2.1.2 explains the system's selected bandwidth and center frequency. Section 2.1.3 introduces the 16-symbol modulation scheme and describes the implementation. Table 2.1 summarizes the design choices for the high-M-ary FSK transmitter.

2.1.1 Transmitter Hardware

The basis of this high-M-ary FSK transmitter design is the rapidly tunable Finisar laser. The Finisar S7500 tunable laser is a MG-YTL integrated with a semiconductor optical amplifier (SOA) that supports 89 channels at 50-GHz spacing to cover the full ITU C-band [9]. The most relevant specifications of this device are listed in Table A.1

Table 2.1: 16-FSK Transmitter Design Characteristics

Hardware Control	
SPI-Bus Clock Rate	42 MHz
Length of (Laser Frequency-Switching) Command	32 bits
Laser-frequency Switching Rate (Theoretical)	1.31 MHz
Optical Design	
Total Optical Bandwidth	15 GHz
M (Number of Symbols)	16 symbols
Optical Frequency Spacing	937 MHz
Overall	
Maximum FSK Symbol Rate (Experimental)	250 KHz
Bits per Frequency Symbol	4 bits
Total Bit Rate	1 Mb/s

in Appendix A.

The Finisar laser takes five input currents to control the SOA, the gain, the left mirror, the right mirror, and the phase-adjust section. The reflector currents adjust the left and right mirrors of the laser, which is useful for coarse and cross-channel tuning. The phase current, in contrast, is more sensitive and can be used to achieve the fine tuning necessary for the implementation of this FSK transmitter.

The laser and laser control setup for operating all functions of the Finisar MG-YTL includes the following devices and controllers:

- Tunable Laser (Finisar S7500)
- Laser Diode and Temperature Controller (Wavelength Electronics LDTC0520)
- 5-Channel Current-Source SoftSpan DAC (Analog Devices LTC2662)
- Microcontroller (Arduino Due)

Fig. 2-1 depicts how these devices interface with each together. The laser device and corresponding temperature controller will be powered using the laser diode driver and thermal controller. Fast and reliable current control of the laser device is achieved using the 5-channel current-source DAC and analog-to-digital converters (ADC), which is interfaced to through the Arduino microcontroller. The Arduino microcontroller selected is the Arduino Due, as it supports a clock speed (84 MHz) and has 512 KB of flash memory, both of which are necessary to run the LTC2662 at fast as possible.

All information, including the test bit sequence, is hard-coded into the Arduino Due's flash memory, allowing a minimum of clock cycles to read and command to the DAC.

Since the upper limit of the LTC2662 SPI serial interface clock speed is 50 MHz [6], I operate the Arduino at 42 MHz. At 32 bits per command, including the one to change the phase current, thus fine-tuning the frequency, this offers a theoretical maximum laser-frequency switching rate of 1.31 MHz. Due to the specific and undisclosed implementation of the official Arduino SPI library, there exists additional dead time that results in frequency-switching on the order of 4 ns, leading to a realizable switching rate of 250 KHz.

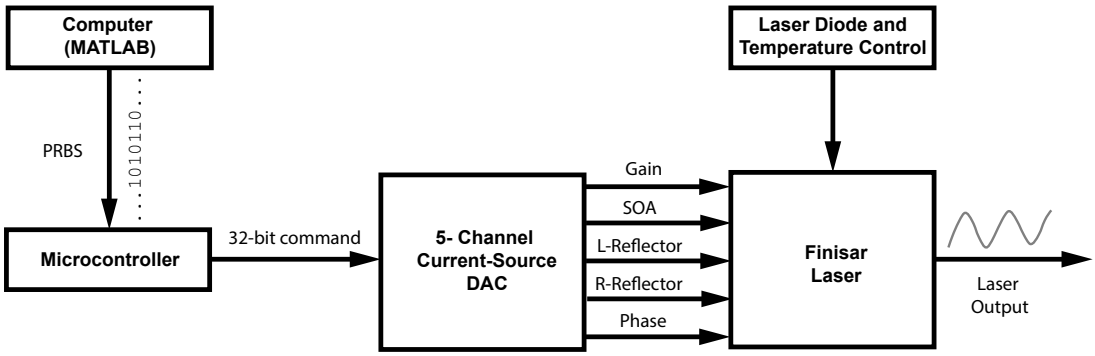

Figure 2-1: FSK Transmitter System Diagram

2.1.2 Receiver Bandwidth

To fit within the bandwidth of a conventional photo-receiver, the transmitter output is accordingly limited to 10 – 20 GHz. This matches the bandwidth of the Discovery Semiconductor R413 dual-polarization coherent receiver that was chosen to use for demodulating the FSK waveforms. Fig. 2-2 illustrates the experimental receiver setup used to calculate the bit error ratio (BER). A dual-polarization coherent receiver generates I/Q signals from the mixing of the laser input and the local oscillator. The carrier frequency of these signals is recorded on a high-bandwidth, real-time oscilloscope, a DSA91304A Infiniium Oscilloscope. This waveform data is processed separately in MATLAB to recover the original frequency symbol and corresponding

bit sequence. This recovered bit sequence is processed in Python to determine the bit-error ratio.

The experimental receiver implementation introduces many constraints on the design of this FSK transmitter. The final design centers a 15-GHz bandwidth around 1545.23 nm, or 194.146 THz. This center wavelength is determined based on the reference mode options provided by the local oscillator, a ClarityPlus tunable laser, and corresponds specifically to the P-branch 4 absorption line [7]. The reference-lock mode is critical in keeping the local oscillator stable to within <0.1 pm. Having predetermined the center wavelength, the left and right reflector currents can be adjusted to find a channel that matches this center wavelength. Once 1545.23 nm is near the center of the channel, the fine-adjust phase currents can be used to fine tune and switch between frequency symbols. The currents used to control the Finisar laser can be found in Table 2.2, where the output current is calculated using the equation $I = n/(2^{16} - 1) \times span$.

Table 2.2: Current Specifications Used in Finisar Laser Control

Current Type	Max Current Out (span)	16-bit Value (n)	Output Current (I)
SOA	100 mA	60000	91.5 mA
Gain	100 mA	60000	91.5 mA
Left Mirror	25 mA	2000	0.763 mA
Right Mirror	25 mA	7500	2.86 mA
Phase Range	6.25 mA	17500 - 28500	1.67 - 2.72 mA

I also constrained the bandwidth to 15 GHz due to unexpected distortions in the Finisar laser output caused when frequency-switching rates exceeded 100 KHz. At this rate, the phase current is no longer able to perform fine-tuning at the edges of the frequency range, leading to hopping across channels. This in turn causes the carrier frequency to be too high for the real-time oscilloscope to capture the waveform, prohibiting demodulation of the signal.

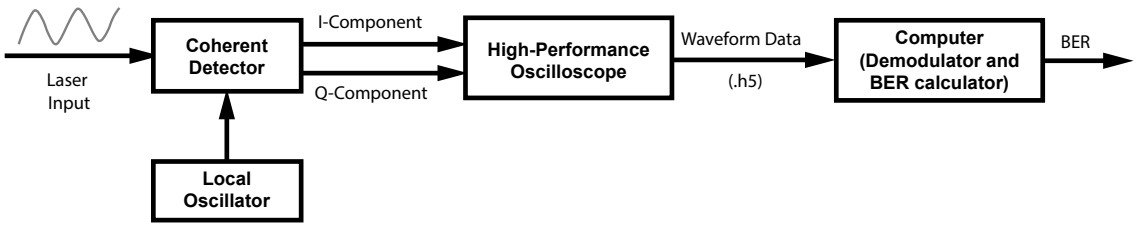

Figure 2-2: FSK transmitter test receiver diagram.

2.1.3 Symbol

Although the local oscillator is stable, the Finisar laser output is still prone to slight wavelength fluctuations. These fluctuations are only on the order of 0.1 – 0.3 pm, but they make it impossible to implement a 256-FSK (or 8 bits/symbol) modulation scheme due to inadequate frequency spacing. This behavior is illustrated in Fig. 2-3, which shows experimental histograms observed from the laser's output at certain symbol setpoints. A 16-FSK modulation scheme was chosen for implementation, because it provides adequate frequency spacing and was easy to extend to the current byte structure used for data processing. With a 16-FSK modulation scheme, each frequency symbol represents four bits, which is defined here as a nibble. Refer to Fig B-1 for a brief summary of the nibble architecture chosen for implementation, and Table A.2 for the corresponding phase counts for each symbol.

2.2 Data Specifications

Section 2.2.1 explains how to generate the pseudo-random symbol sequence used to test the FSK transmitter. Section 2.2.2 explains how the corresponding sequence of symbols would instead be generated from actual data.

2.2.1 PRBS Generation

To test the performance of communication systems, it is best to use a long sequence of bits that appears as random as possible. In the field of telecommunications, statistical randomness can be simulated using a pseudo-random bit sequence (PRBS) generated

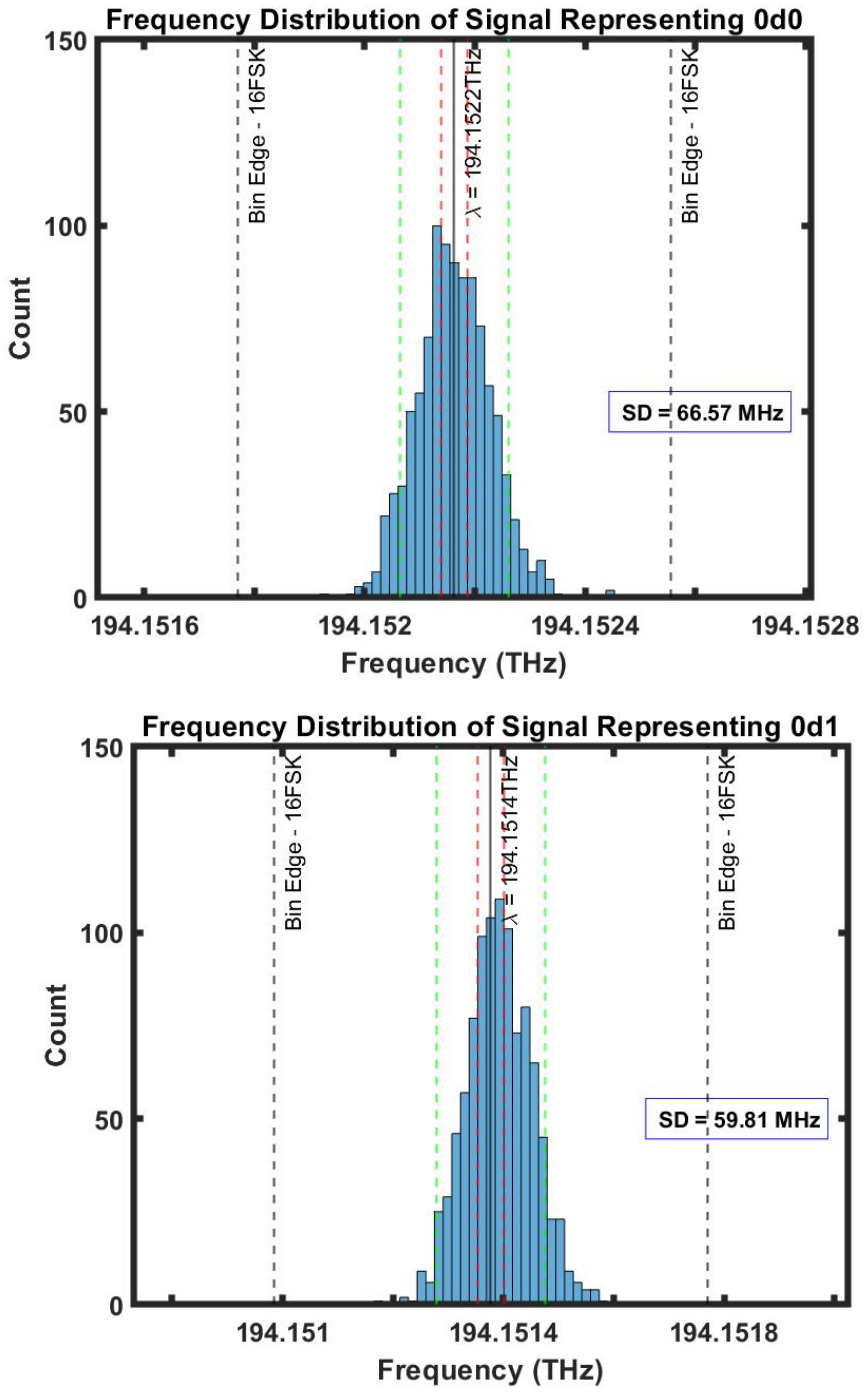

Figure 2-3: Histograms of the frequency distribution of symbols `0d0` and `0d1`. The solid line represents the target frequency output by the laser. The dotted lines refer to the edge of the frequency binning range corresponding to a particular M-FSK. Black: 16-FSK limits. Green: 64-FSK limits. Red: 256-FSK limits.

by linear shift registers [8]. For this performance characterization, I tested four PRBS-k sequences. The monic polynomials that generate these four PRBS-k sequences are as follows:

$$\text{PRBS-6} = x^6 + x^5 + 1 \quad (63 \text{ bits})$$

$$\text{PRBS-7} = x^7 + x^6 + 1 \quad (127 \text{ bits})$$

$$\text{PRBS-8} = x^8 + x^6 + x^5 + x^4 + 1 \quad (255 \text{ bits})$$

$$\text{PRBS-9} = x^9 + x^5 + 1 \quad (511 \text{ bits})$$

These monic polymials generate a bit sequence of $2^k - 1$ bits, which I then converted to a $2^k - 1$ symbol sequence using a methodology depicted in Fig. 2-4. As this is not actual data, but instead a self-determined test sequence, this methodology should have no effect on the resulting bit-error ratio measurements.

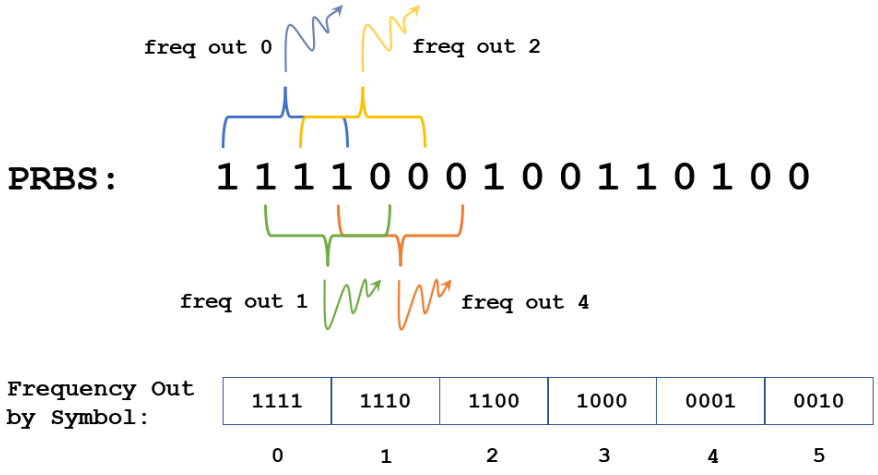

Figure 2-4: Creation of pseudorandom symbol sequence using example PRBS in 16-FSK encoding. The test symbol sequence that would have been transmitted and received is shown at the bottom.

2.2.2 Data Handling

Shown in Fig 2-5 is the bit sequence to frequency symbol conversion that is used with actual data. Note that each delineated position corresponds to a nibble.

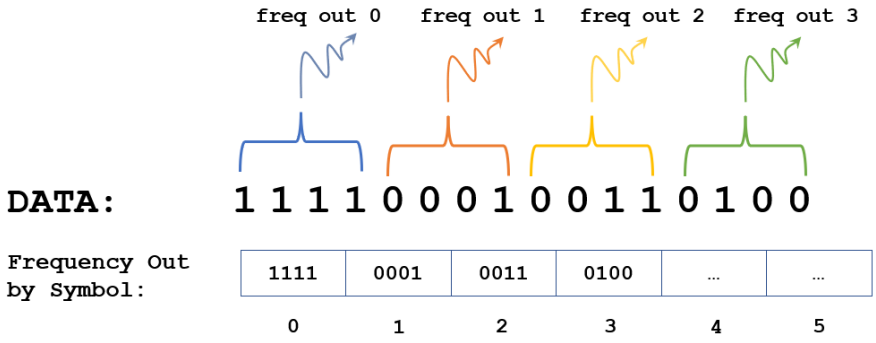

Figure 2-5: Creation of output symbol sequence when using actual data

Chapter 3

Performance Analysis

The performance of the 16-FSK transmitter is evaluated using bit-error ratio (BER) measurements, which compares how accurately a predefined bit sequence can be produced by the transmitter and demodulated by the receiver. The BER quantity is the ratio of bit errors detected to total bits sent. The BER was assessed for the different sequences of the varying lengths described in Sec. 2.2.1. For a combination of predetermined PRBS sequences, the total aggregate bits were detected by the receiver and compared to the bit pattern sent, allowing the BER value to be calculated for each test condition. For example, the test pattern might include 16 runs of the PRBS-6 sequence and 2 runs of the PRBS-9 sequence. This allows for a maximum number of bits that can be manageably analyzed by the analysis routine. The BER measurement results are presented in Sec. 3.1. While assessing the BER performance, repetitions of previous symbols were consistently observed at semi-regular occurrences in the FSK waveforms. Sec. 3.2 describes more details of these duplicate symbols, as well as investigates their root causes.

3.1 Bit-Error Ratio (BER)

Table 3.1 summarizes the calculated BERs of all four PRBS-k sequences. These BERs are calculated while skipping over each occurrence of duplicate symbols, as including every duplicate leads to BERs that are unrealistically high and are possibly an artifact

of the control and pattern-generation techniques. For example, a PRBS-6 sequence of length 63 has an average of 4 duplicates per run, while a PRBS-9 sequence of length 511 has an average of 38 duplicates per run.

Over all the test cases performed, the BERs for the PRBS sequences fall between 0.20% – 0.35%. Many error-free transmissions (sequence runs where there were zero bit errors) were achieved. Error-free performance occurred for 10 of the 16 test runs with the PRBS-6 pattern, three of the eight PRBS-7 test runs, and two of the four PRBS-8 test runs. The other test runs did exhibit errors, and these errors were tabulated over the total number of tests performed for each PRBS pattern and used to calculate BER values. Table 3.1 summarizes the BER performance for the 16-FSK transmitter using the MG-YTL source. The BER generally on the order of 1×10^{-3} for the different cases studied.

Table 3.1: BER Across Different PRBS Sequences (Ignoring Duplicates)

PRBS-k	Total Bits Analyzed	Total Bit Errors	Bit Error Ratio
PRBS-6	4032	12	2.98×10^{-3}
PRBS-7	4064	15	3.69×10^{-3}
PRBS-8	4080	8	1.96×10^{-3}
PRBS-9	4088	9	2.20×10^{-3}

An investigation into the sources of the bit errors was performed to develop further insights into the FSK transmitter's performance. It was theorized that errors could result from the high frequency-switching rates applied to the laser from the digital logic driving the MG-YTL. There is a possibility that the fast frequency-switching rate causes distortions in more areas than just at the edges of the frequency ranges. In light of this, slowing the SPI clock frequency down was investigated to identify if glitches in the symbols were resulting from the drive logic. Experiments were done with a reduced SPI serial interface clock speed, decreasing this from 42 MHz to 21 MHz. However, this change did not demonstrate any significant improvement in the BER, and actually increased errors were observed with this decreased clock speed of 21 MHz, as seen in Table 3.2. This could have resulted from increased laser wavelength drift over the longer symbol periods, or from lower resolution in the

symbol slot time. Higher SPI bus frequencies would be worth investigating to see if the BER continues to decrease. However, the 42-MHz SPI bus rate is the fastest rate that the current microcontroller and DAC hardware can support.

Table 3.2: Six PRBS-9 Sequences Tested at Different SPI Clock Speeds

SPI Clock Speed	Total Bits	Average # of Duplicates	BER (Without Duplicates)
42 MHz (original)	12,264	38	2.53×10^{-3}
21 MHz (test)	12,264	40	4.73×10^{-3}

Histograms showing the frequency distribution for each symbol used in the 16-FSK transmitter were also collected and analyzed, and these are provided in Figs. B-4 – B-17 in Appendix B. These distributions show that some symbols have wider distributions than others, which could be responsible for some of the errors. These are static distributions taken at the baseline SPI clock frequency, and don't reflect subsequent pattern-dependent effects that could also lead to wavelength excursions that cause errors.

Based on the data-analysis approach, the source of bit errors could also be attributed to the receiver setup. The receiver methodology is currently heavily human-dependent, and the relevant waveform duration must be isolated and saved manually to a file from the real-time scope. There is currently no automated routine to identify the start of each PRBS sequence, but doing so could help with improving consistency in the temporal cropping performed on each waveform collection.

3.2 Symbol Duplication

During the experiments and analysis, an unexpected phenomenon of repeating symbols occurred. It was observed that these duplicates would immediately follow a preceding nibble, and would occur at quasi-regular intervals within the PRBS patterns. The diagram in Fig. 3-1 shows how the duplicate symbols were typically observed in the experiments.

The behavior of the duplicates, especially their distribution as seen in Fig 3-2,

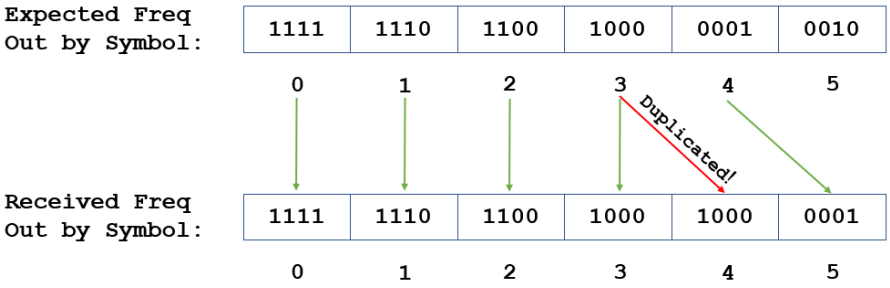

Figure 3-1: Typical behavior of symbol duplicates that occur during transmission of PRBS data sequences.

makes it difficult to ascertain their root cause. While these duplicates may occur in semi-regular intervals, there is no deterministic pattern either considering the sequences altogether or sequence by sequence. In each single PRBS sequence, the gap between subsequent duplicates can be anywhere from 12 – 15 nibbles, indicating a systematic issue with either the digital controller or DAC hardware.

It is unlikely that the duplicates are attributed to the high rate of frequency-switching, as they are not eliminated or significantly reduced as a result of halving the clock speed as shown in Table 3.2. The most likely source of these duplicates appears to be unexplained delays occurring in the microcontroller that cause stale bits to be transferred to the DAC, whether it is between sending commands, or during the sending of a command. The sequence resumes correctly after a duplicate occurs and there are minimal extra errors, implying that these duplicates don't arise from a buffer "misread" on the part of the 5-channel current-source DAC.

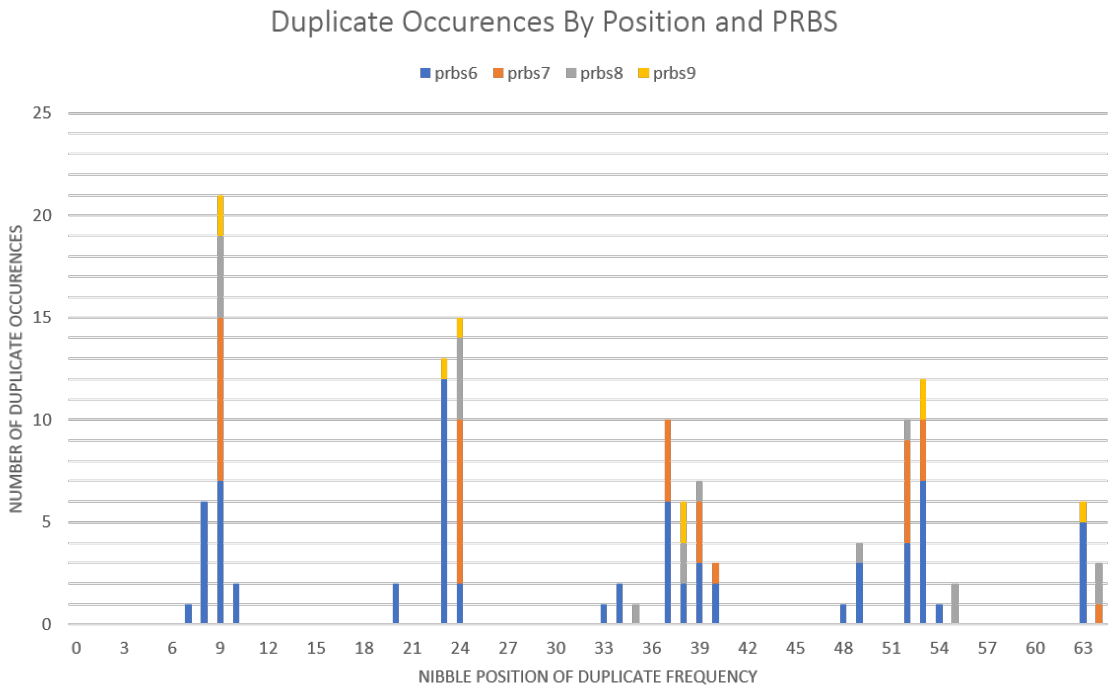

Figure 3-2: Distributions of the symbol duplicate occurrence in the first 64 received symbols for all the PRBS patterns tested.

Chapter 4

Reflections & Observations

4.1 Challenges

There were a lot of technical challenges encountered over the course of this thesis project. A few of these have already been described in the preceding sections alongside the design choices covered in Chapter 2, such as bandwidth limitations caused by high-speed frequency-switching, spread in frequency distributions for the different symbols, and other likely causes for bit errors. There were also a few technical challenges encountered both before and after that phase of the project.

Before the high-speed frequency-switching was possible, I first needed to create the lookup table that would match each frequency symbol to its corresponding target frequency, which can only be done by spanning the phase range and manually recording the wavelength value corresponding to each tested phase setpoint. I was able to greatly simplify this process by using MATLAB to automate (1) setting the phase count, (2) communicating with the oscilloscope to save the waveform data at that point in time, and (3) calculating the average frequency of that saved waveform using the beat tone from the LO. With this one can easily create a plot of phase current count versus wavelength, and use curve fitting techniques to calculate the target frequency for each frequency symbol.

After implementing the PRBS pattern transmission, I was confronted with an additional technical challenge and a human limitation. I was incapable of easily dis-

tinguishing between MHz-scale frequencies on the oscilloscope with the naked eye, and could not precisely determine where a transmitted PRBS sequence began. However, doing so was critical to the frequency demodulation routine and to enable the BER calculations from the predetermined PRBS patterns. It felt like divine intervention when I remembered that going beyond my phase current range had the effect of hopping channels, something that resulted in a flat line on the oscilloscope because the signal was out of band of the receiver electronics. While one cannot easily distinguish between MHz-scale frequencies on a scope, one can readily identify a flat line from an in-band signal. By forcing a few large channel hops prior to the start of each PRBS sequence, one could readily determine where the signal starts, and pinpoint the start of each PRBS sequence. A visual example of this approach is provided in Fig. B-3 of Appendix B.

4.2 Future Work

While the receiver data collection process is not currently automated, the process of automating it could be rather straightforward to implement. Instead of using visual cues to determine where the start of a sequence is, one could extend the microcontroller's current capabilities to indicate when a signal is transmitting, sending out 0 V when during a pattern and +3.3 V when a pattern is not being transmitted. By connecting this indicator to the oscilloscope, one could use the advanced trigger option to set the location of the start of the signal in the waveform memory. This would eliminate the need to hop channels to visually indicate the start of a new pattern.

In addition, there were some latencies that occurred due to undocumented behaviors of fundamental Arduino libraries. In particular, the theoretically-achievable 1.31-MHz frequency-switching rate was not realizable with the current hardware setup, and instead the maximum switching rate that could be achieved was only 250 KHz. Such uncertainties in the digital control could be eliminated by switching to field-programmable gate arrays (FPGAs), that exhibit more deterministic and predictable performance. This would allow the bit sequences to be dynamically converted into the

correct frequency symbol sequences in a more real-time manner. An FPGA approach may also eliminate problems with duplicate symbols as observed in the current setup.

Once the channel hopping approach is eliminated (the cause of the flat lining on the oscilloscope) and dynamic generation of frequency symbols is enabled, the experimental setup could then be configured to transmit actual data over a link.

Further work could also be done to operate multiple 16-FSK transmitters. For example, it is possible to integrate two 16-FSK setups into one, as it would be possible to have the microcontroller and the real-time oscilloscope accommodate a second 16-FSK signal generation and signal collection. For such a 2x16-FSK approach, the waveforms could be sufficiently out of band with each other and two different LOs could be be used to demodulate each parallel waveform. Alternatively, 16-FSK transmitter could be used to enhance the maximum data rate of other modulation schemes such as PPM, as the FSK modulation's time independence allows the two modulation schemes to coexist simultaneously. Finally, digital signal-processing approaches could be developed to detect the waveform in real-time and directly deconvolve the data pattern from the discrete frequency shifts.

Chapter 5

Conclusions

In the early part of this thesis project, a 256-FSK modulation scheme was envisioned based on the bandwidth of the receiver and frequency jumps that the Finisar MG-YTL could achieve based on it's manufacturer specifications. However, limitations of the Finisar tunable laser, LO laser accuracy and stability, wave-meter measurement accuracy, and microcontroller buffer constraints led to a demonstration of a 16-FSK transmitter approach using a fast tunable laser. Good BER performance was demonstrated for different PRBS patterns, and limitations related to the microcontroller and hardware setup were identified. Addressing these limitations could likely result in >Mb/s-class, error-free transmission of 16-FSK waveforms.

Scaling to 256-FSK with this approach could still be achieved using a number of possible improvements that have been discussed previously in this thesis. For example, implementing two 16-FSK transmitters in parallel would be one option, while another option could be using an enhanced bandwidth photo-receiver and detection electronics, and FPGA-based controllers. These approaches would still provide a significant reduction in hardware complexity over a conventional 256-FSK transmitter using discrete laser sources and multiple consecutive filter blocks [4]. FSK modulation offers power efficiencies comparable to PPM modulation and hardware simplicity, and the use of multiple FSK sources alongside coherent detection overcomes PPM's electrical bandwidth limitations and timing-resolution constraints. As the capabilities of tunable lasers and laser controllers increase, whether it be in greater output stabiliza-

tion, faster frequency-switching rates, or smaller frequency jumps, the capabilities of tunable-laser-based FSK systems will also increase. This work has shown that FSK modulation schemes are a promising method to implement electrically-bandwidth efficient waveforms with low hardware complexity, and is an approach that scales well to data rates well beyond what is demonstrated in this work.

Appendix A

Tables

Table A.1: Finisar S7500 Laser Characteristics, per Datasheet in Ref. 9.

ATTRIBUTE	SYMBOL	MIN	TYP	MAX	UNITS
Operating Currents					
Gain	I_g		98	100	mA
Reflector	I_{rl}, I_{rr}			33	mA
Phase	I_p			7.5	mA
SOA	I_{SOA}			167	mA
Temperature and Thermistor Characteristics					
Current	I_{TEC}		<0.75	0.85	A
Voltage	V_{TEC}		<2.5	2.8	V
Thermistor Resistance	R_{th}		10		kΩ
Laser chip temperature	T_L	25		30	°C
Optical Characteristics					
Output Power	P_{max}	13			dBm
Side-mode suppression ratio	$SMSR$	40			dB
Optical signal-to-noise ratio	$OSNR$	50	55		dB
Linewidth	LW			5	MHz
Lowest emission wavelength	λ_{min}	1527.6	1528.8		nm
Highest emission wavelength	λ_{max}		1563.9	1568.4	nm

Table A.2: Nibble to Phase Count Conversion as per 16-FSK Modulations

SYMBOL #	BINARY	WAVELENGTH (nm)	PHASE COUNT
0	0000	1545.1798	28273
1	0001	1545.18605	27674
2	0010	1545.1923	27072
3	0011	1545.19855	26469
4	0100	1545.2048	25865
5	0101	1545.21105	25261
6	0110	1545.2173	24657
7	0111	1545.22355	24053
8	1000	1545.2298	23449
9	1001	1545.23605	22848
10	1010	1545.2423	22248
11	1011	1545.24855	21650
12	1100	1545.2548	21055
13	1101	1545.26105	20462
14	1110	1545.2673	19875
15	1111	1545.27355	19291

Appendix B

Figures

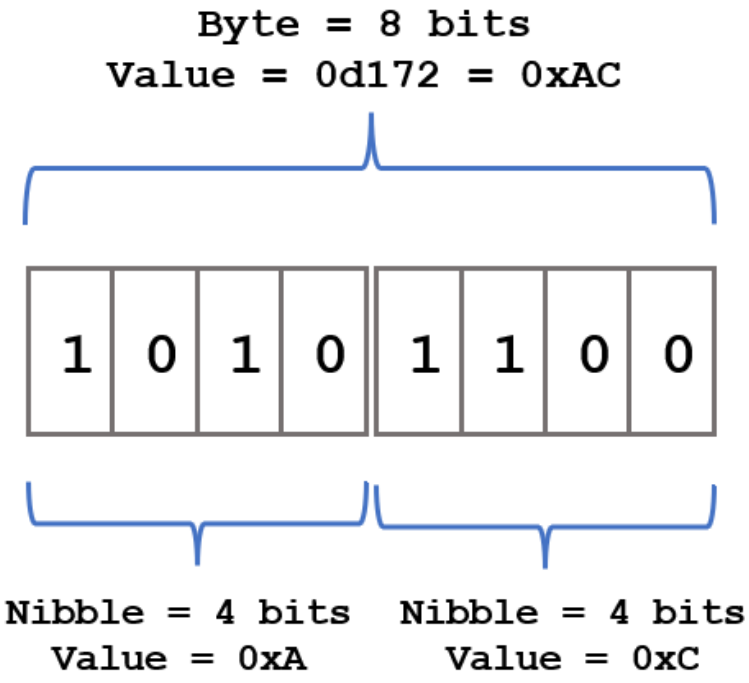

Figure B-1: Overview of the nibble architecture

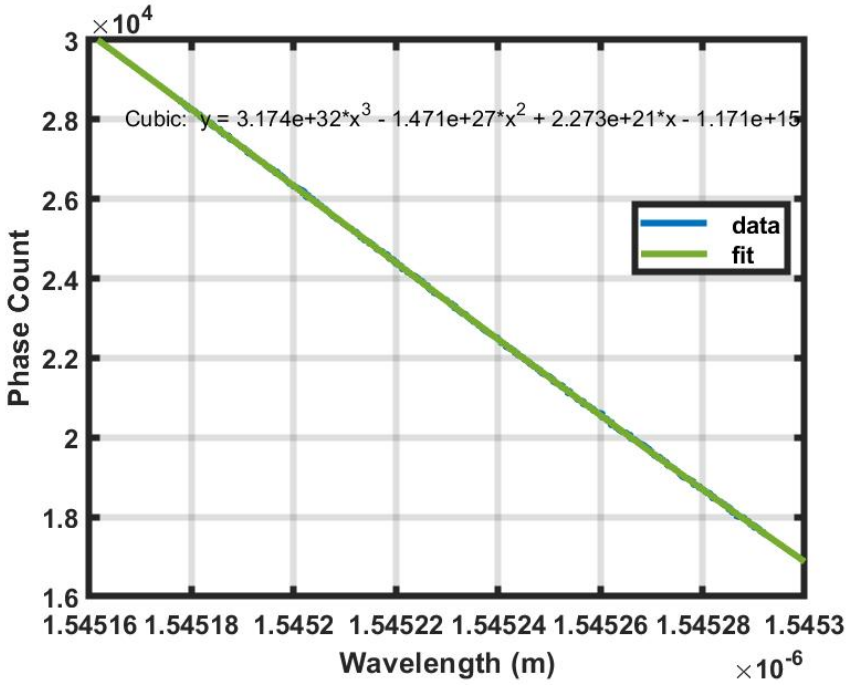

Figure B-2: Plotted data and fit line of desired wavelength to phase count conversion.

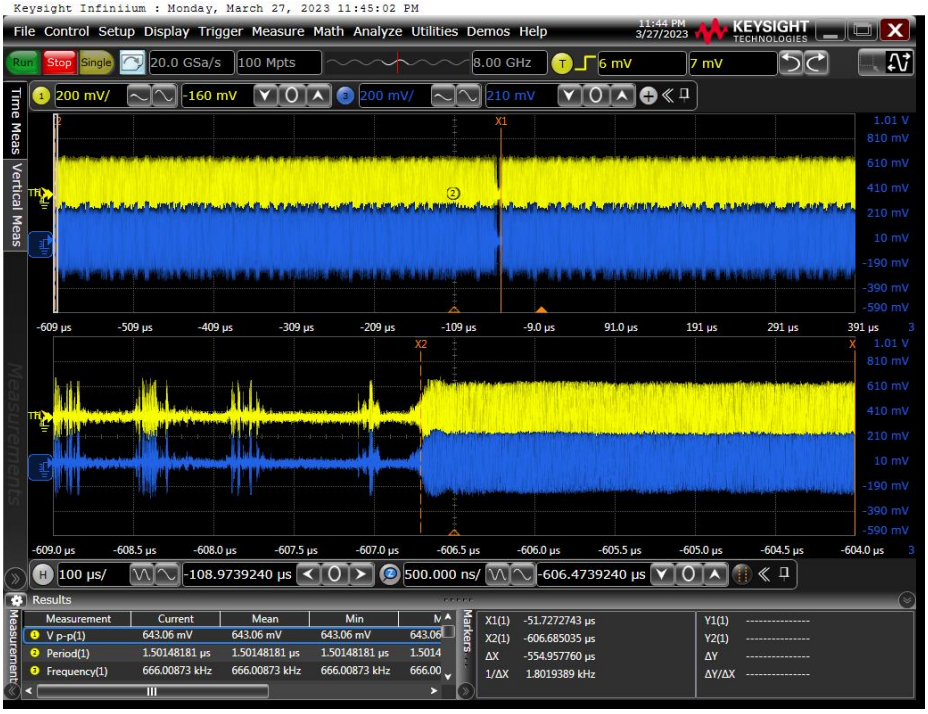

Figure B-3: Example oscilloscope visual of the I/Q signals outputted by the coherent receiver.

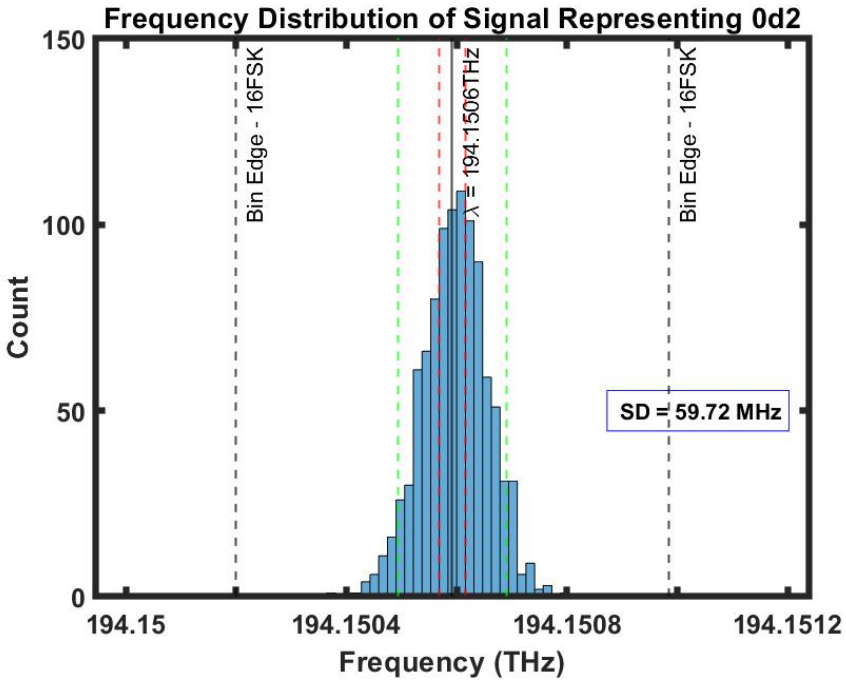

Figure B-4: Histogram of symbol 0xD2.

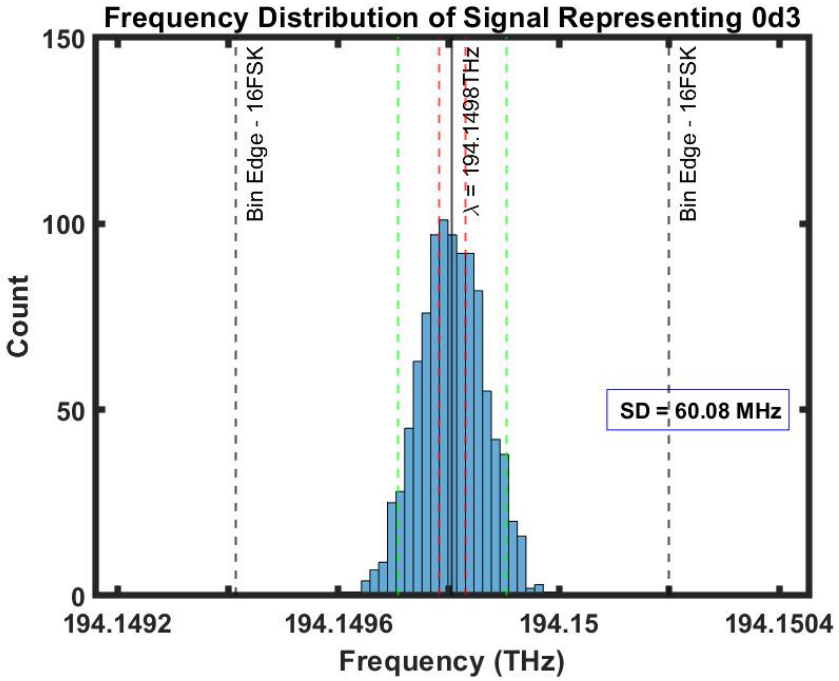

Figure B-5: Histogram of symbol 0xD3.

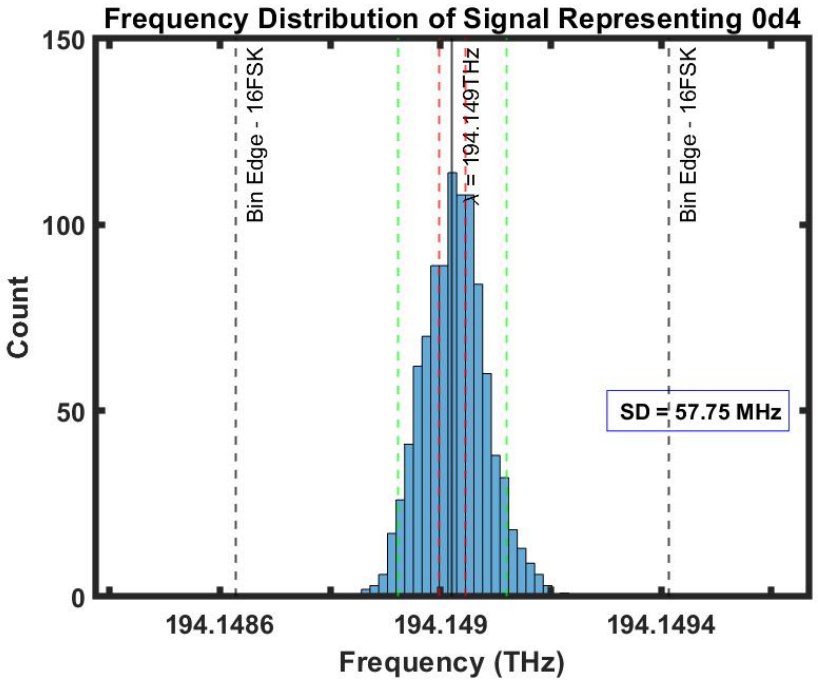

Figure B-6: Histogram of symbol 0xD4.

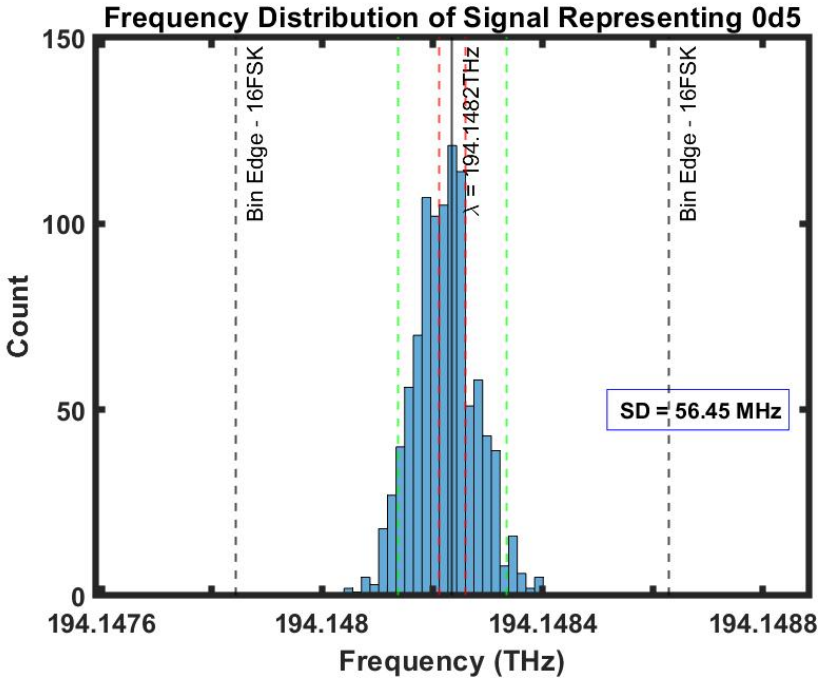

Figure B-7: Histogram of symbol 0xD5.

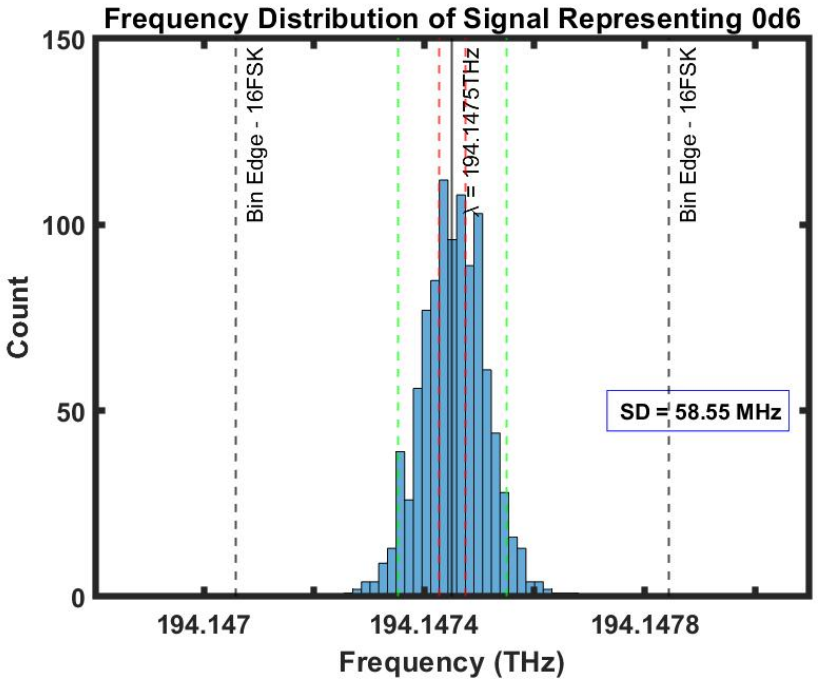

Figure B-8: Histogram of symbol 0xD6.

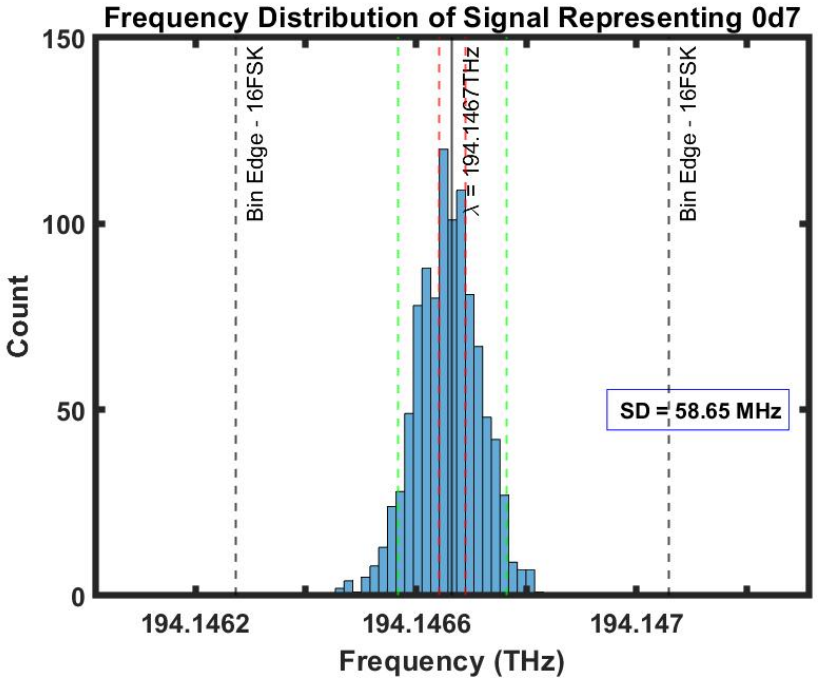

Figure B-9: Histogram of symbol 0xD7.

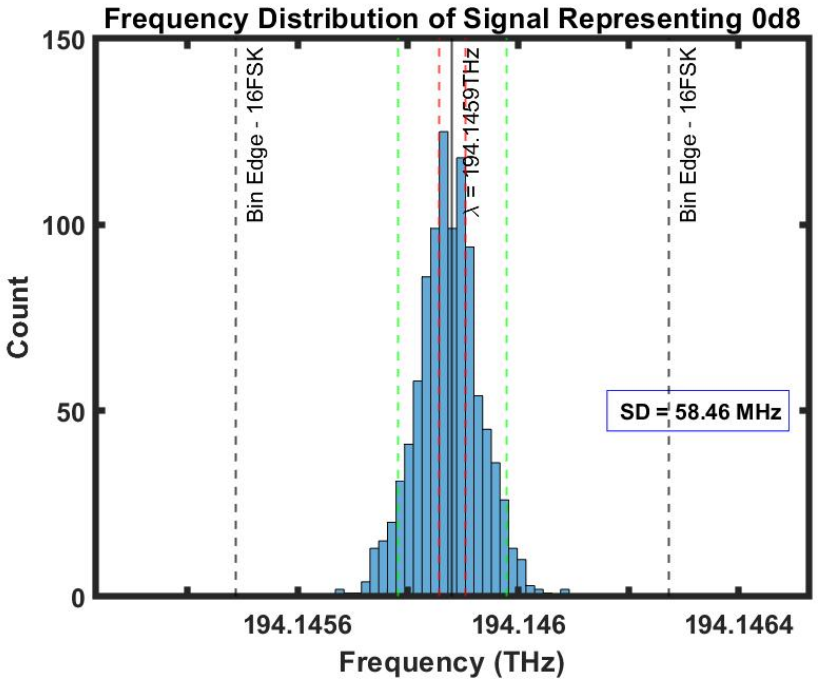

Figure B-10: Histogram of symbol 0xD8.

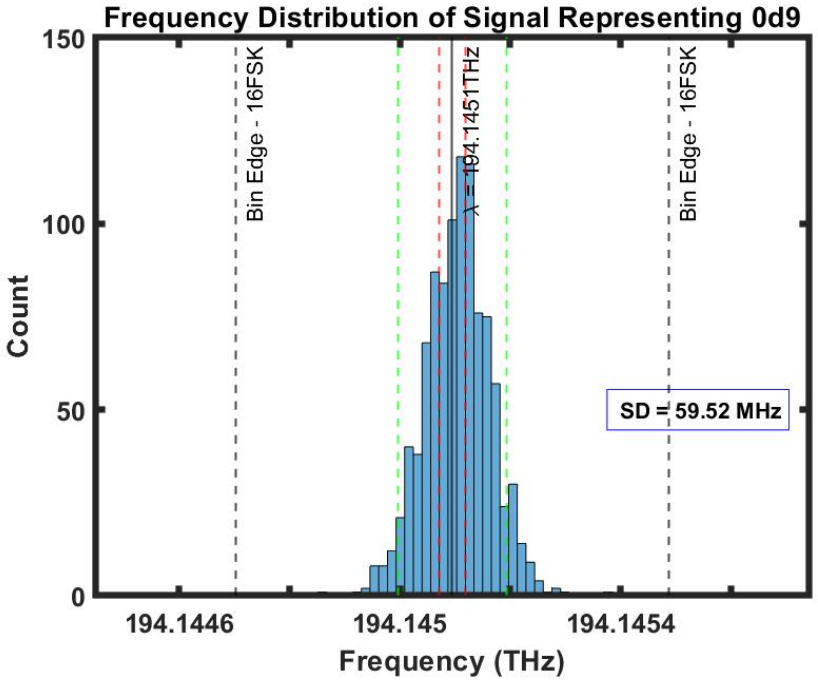

Figure B-11: Histogram of symbol 0xD9.

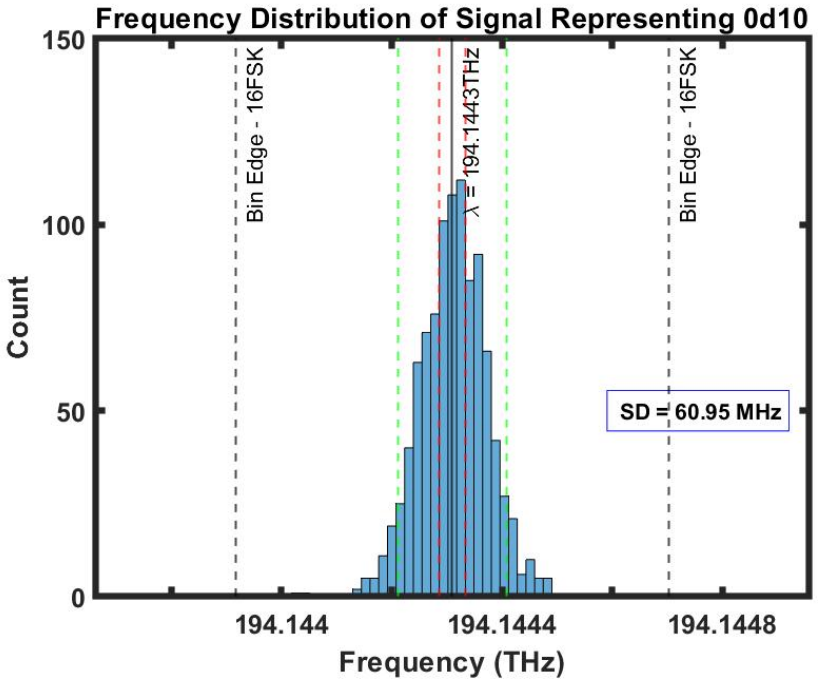

Figure B-12: Histogram of symbol 0xDA.

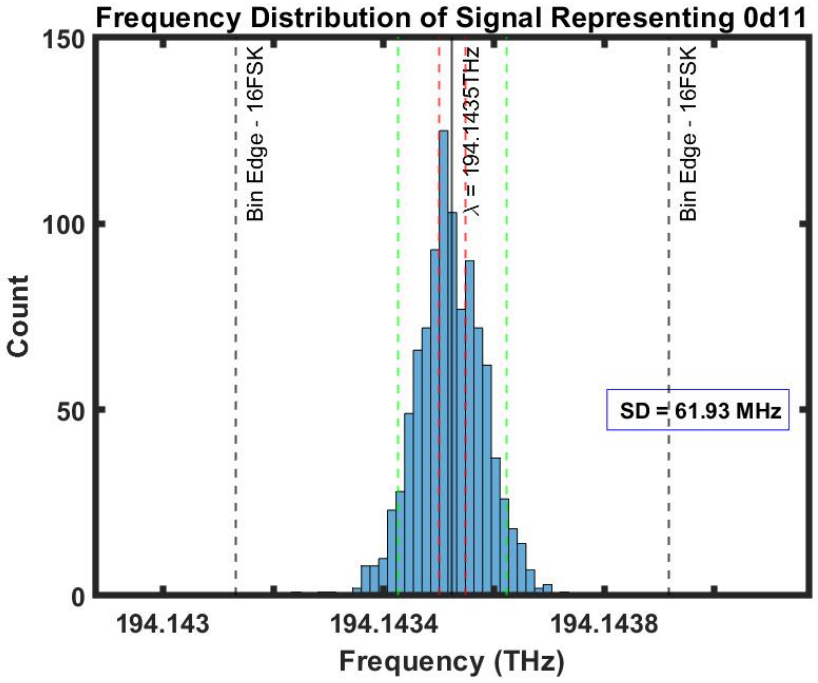

Figure B-13: Histogram of symbol 0xDB.

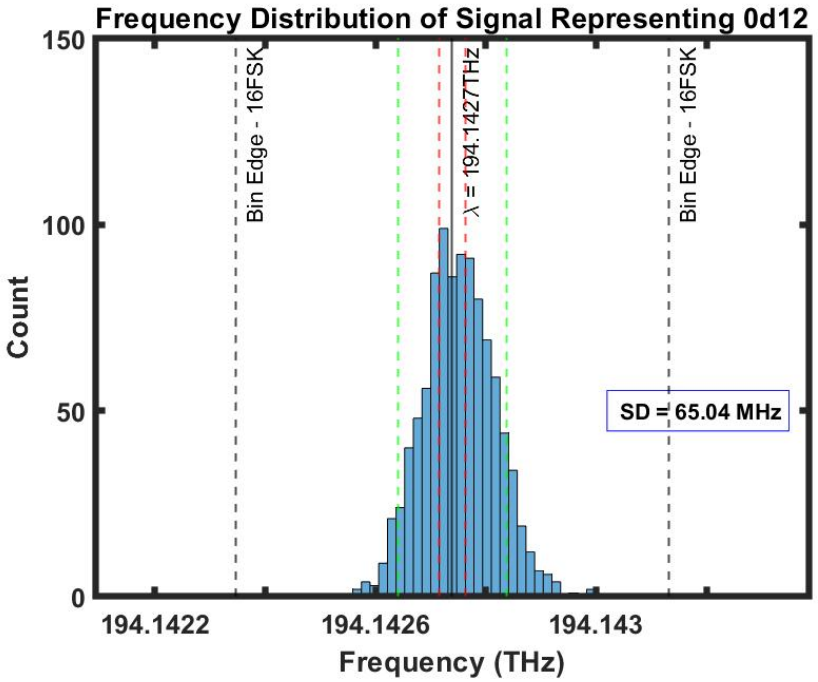

Figure B-14: Histogram of symbol 0xDC.

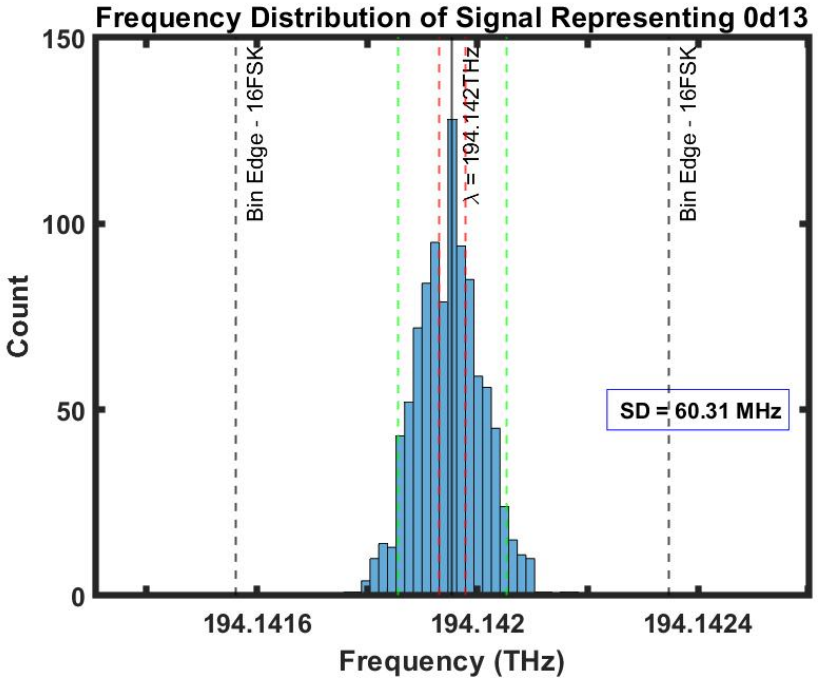

Figure B-15: Histogram of symbol 0xDD.

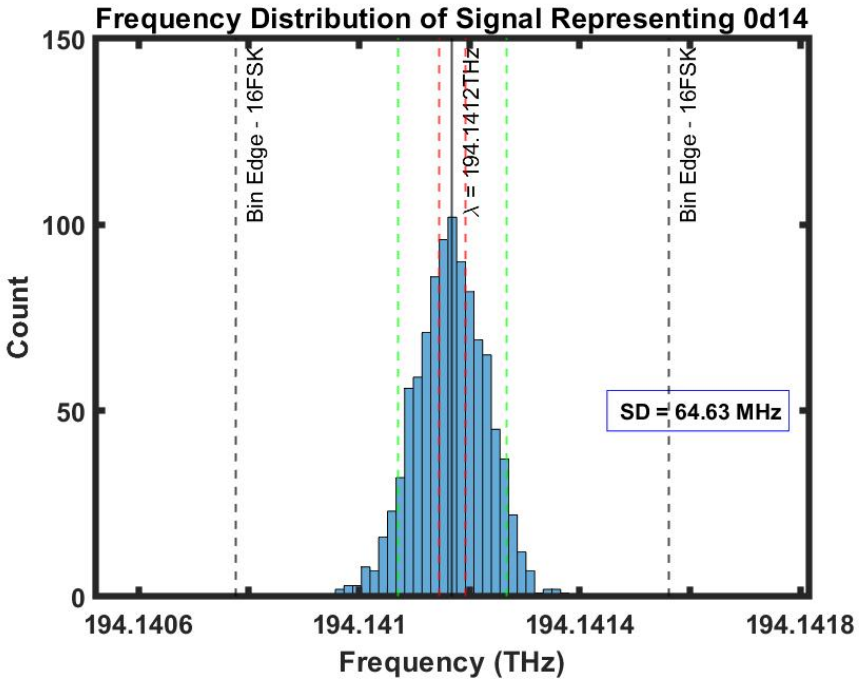

Figure B-16: Histogram of symbol 0xDE.

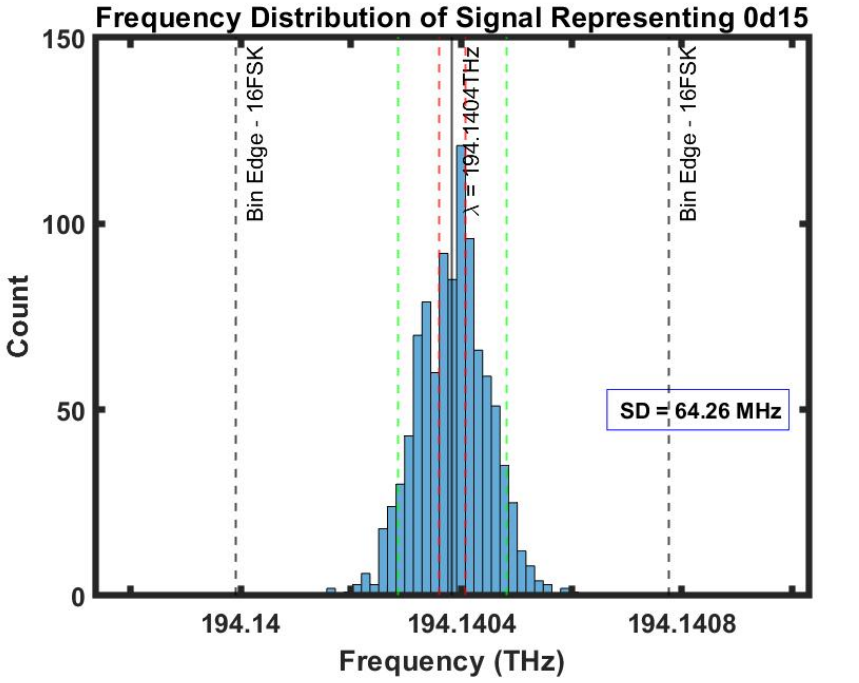

Figure B-17: Histogram of symbol 0xDF.

Bibliography

[1] Frank Heine, Patricia Martin-Pimentel, Nils Höpcke, David Hasler, Christoph Rochow, and Herwig Zech,"Status of Tesat Lasercomms activities," Free-Space Laser Communications XXXIII, SPIE Photonics West, paper 116780C, Ed. Hamid Hemmati and Don M. Boroson, Feb. 2021.

[2] Chaudhry, Aizaz U. and Yanikomeroglu, Halim, *IEEE Vehicular Technology Magazine*, "Laser Intersatellite Links in a Starlink Constellation: A Classification and Analysis," **16**(2), pp. 48–56, 2021.

[3] Boroson, Don M. (67). 2005. Optical Communications: A Compendium of Signal Formats, Receiver Architectures, Analysis Mathematics, and Performance Characteristics. MIT-LIN-ZZZ-05155. Unclassified

[4] Shelby Jay Savage, Bryan S. Robinson, David O. Caplan, John J. Carney, Don M. Boroson, Farhad Hakimi, Scott A. Hamilton, John D. Moores, and Marius A. Albota, "Scalable modulator for frequency shift keying in free space optical communications," Opt. Express 21, 3342-3353 (2013).

[5] M. Mestre, J. M. Fàbrega, J. A. Lázaro, V. Polo, A. Djupsjöbacka, M. Forzati, P. -. Rigole, and J. Prat, "Tuning Characteristics and Switching Speed of a Modulated Grating Y Structure Laser for Wavelength Routed PONs," in Advanced Photonics & Renewable Energy, OSA Technical Digest (CD) (Optica Publishing Group, 2010), paper AThC2.

[6] Analog Devices, “Five-Channel, 300mA Current-Source Output 16-/12-Bit Soft-Span DACs," LTC2262 datasheet, [Revised Jan. 2019].

[7] Wavelength References, "ClarityPlus™ Precision Frequency Standard Full C Band Tunable Laser," ClarityPlus datasheet, [Revised 2019].

[8] Paul H. Bardell, William H. McAnney, and Jacob Savir, "Built-In Test for VLSI: Pseudorandom Techniques", John Wiley & Sons, New York, 1987.

[9] Finisar Corporation, “CW Tunable Laser – Butterfly Package," S7500 datasheet, [Dec. 2011].